

The Monitor project: the search for transits in the open cluster NGC 2362

Adam A. Miller^{1,2*}, Jonathan Irwin^{1,3}, Suzanne Aigrain⁴, Simon Hodgkin¹, Leslie Hebb⁵.

¹*Institute of Astronomy, University of Cambridge, Madingley Road, Cambridge, CB3 0HA, United Kingdom*

²*Astronomy Department, University of California at Berkeley, Berkeley, CA 94720-3411, USA*

³*Harvard-Smithsonian Center for Astrophysics, 60 Garden Street, Cambridge, MA 02138-1516, USA*

⁴*Astrophysics Group, School of Physics, University of Exeter, Stocker Road, Exeter, EX4 4QL, United Kingdom*

⁵*School of Physics and Astronomy, University of St. Andrews, North Haugh, St. Andrews, KY16 9SS, Scotland*

ABSTRACT

We present the results of a systematic search for transiting planets in a ~ 5 Myr open cluster, NGC 2362. We observed ~ 1200 candidate cluster members, of which ~ 475 are believed to be genuine cluster members, for a total of ~ 100 hours. We identify 15 light curves with reductions in flux that pass all our detection criteria, and 6 of the candidates have occultation depths compatible with a planetary companion. The variability in these six light curves would require very large planets to reproduce the observed transit depth. If we assume that none of our candidates are in fact planets then we can place upper limits on the fraction of stars with hot Jupiters (HJs) in NGC 2362. We obtain 99% confidence upper limits of 0.22 and 0.70 on the fraction of stars with HJs (f_p) for 1-3 and 3-10 day orbits, respectively, assuming all HJs have a planetary radius of $1.5R_{\text{Jup}}$. These upper limits represent observational constraints on the number of stars with HJs at an age $\lesssim 10$ Myr, when the vast majority of stars are thought to have lost their protoplanetary discs. Finally, we extend our results to the entire Monitor Project, a survey searching young, open clusters for planetary transits, and find that the survey as currently designed should be capable of placing upper limits on f_p near the observed values of f_p in the solar neighbourhood.

Key words:

techniques: photometric - surveys - planetary systems - open clusters and associations: individual (NGC 2362) - occultations

1 INTRODUCTION

1.1 Transiting Planets Around a Young Star

The detection of a transiting planet provides a wealth of information which cannot be matched by any other planetary detection method at the moment. There have been over 20 transiting planets detected thus far, and the list is growing rapidly¹. These systems provide the only means for directly measuring a planet's radius. They also provide a means for measuring the inclination of the orbital plane, which in turn removes the $\sin i$ ambiguity of a planet only detected via the radial velocity method. If the host star is bright enough, transiting planets also provide a means for measuring their atmospheric composition when the stellar spectrum, in eclipse (planet behind the star),

is subtracted from the combined-light out of eclipse spectrum of the star plus the planet (Richardson et al. 2007; Grillmair et al. 2007). Additionally, very precise measurements of the time of transit can be used to search for and characterise the orbits of other, sometimes very low-mass, planets in the extrasolar system, because these other planets would slightly perturb the transiting planet's orbit (Agol et al. 2005; Holman & Murray 2005).

Despite the recent success of many transit surveys, there has yet to be an observation of a transiting planet orbiting a PMS hydrogen burning star. In fact, there is a relative paucity of detected planets orbiting any stars at an age less than ~ 100 Myr. Aside from the recent claim of the detection of a planet orbiting TW Hydrae (Setiawan et al. 2008), we are unaware of any detections of a planet orbiting a < 100 Myr hydrogen burning star.

Planets are believed to form in protoplanetary discs where formation and accretion, as well as migration, halt following the dispersal of the disc. Haisch et al. (2001) found

* E-mail: amiller@astro.berkeley.edu (AM)

¹ <http://obswww.unige.ch/~pont/TRANSITS.htm>

that roughly 50% of stars lose their discs by ~ 3 Myr, while nearly all discs are dissipated by ~ 10 Myr. This places a significant constraint on the formation time of a gaseous giant planet at $\lesssim 10$ Myr (Bodenheimer & Lin 2002). The discovery of a planet around a very young star, specifically ~ 5 Myr, would provide important constraints for planetary formation mechanisms, migration time scales and dynamical evolution, and their relation to disc lifetimes and clearing time scales (Bodenheimer & Lin 2002). A transiting planet at ~ 5 Myr would lead to constraints on the planet mass and radius at an early age, i.e. very near the initial conditions for giant planet evolution, which are essentially unconstrained at the moment.

1.2 The Cluster

NGC 2362 is a well studied open cluster whose age (~ 5 Myr; Moitinho et al. 2001, Delgado et al. 2006), which coincides with the tail of the distribution of circumstellar disc lifetimes, and relatively moderate distance (1480 pc, $(m - M)_0 = 10.85$; Moitinho et al. 2001) make it an ideal test bed for the study of stars and their environments during the early pre-main sequence (PMS). For example, the detection of detached eclipsing binary (EB) stars in the cluster will provide measurements of each star’s mass and radius without the use of a model. These measurements can, in turn, be used to constrain PMS evolution models.

Many recent surveys have been conducted to characterise the properties of NGC 2362. The most relevant work includes the determination of fundamental cluster properties (Moitinho et al. 2001), the determination of the circumstellar disc fraction from near-IR excess (Haisch et al. 2001), an H α emission survey to study T Tauri stars and disc accretion (Dahm 2005), and a study of primordial circumstellar discs using infrared excesses measured by the *Spitzer Space Telescope* (Dahm & Hillenbrand 2007).

1.3 The Survey

We have completed a high cadence photometric monitoring survey of NGC 2362, with observations made using the Mosaic II imager on the 4m Blanco telescope at CTIO. There are three primary scientific goals of this survey: one, to discover low-mass EB systems which will allow us to simultaneously measure the mass and radius for each member of the system, two, to search for transiting planets orbiting PMS stars, and three, to characterise the rotation periods for low-mass members of the cluster (Irwin et al. 2008).

Our observations of NGC 2362 were designed to be sensitive enough to detect a large planet ($R_p \gtrsim 1R_{\text{Jup}}$) in a ‘very hot-Jupiter’ orbit, i.e. orbital period $\lesssim 3$ days (Aigrain et al. 2007). Specifically, given the average observational cadence of ~ 6 min during 18 nights spread over a year with optimal signal-to-noise we ought to be able to photometrically detect planets with $R_p > 1R_{\text{Jup}}$ around a $0.7 M_{\odot}$ primary. For lower mass, and hence fainter, stars Aigrain et al. (2007) predicted that we should be able to detect planets with $R_p \gtrsim 2R_{\text{Jup}}$ orbiting a $0.2 M_{\odot}$ primary. This corresponds roughly with the spectroscopic limits from 8 m class telescopes. Aigrain et al. (2007) shows that it would be possible to detect the radial velocity (RV) signal of a $1M_{\text{Jup}}$ planet

orbiting a $0.2 M_{\odot}$ primary in a 1 day orbit down to $I \sim 18$ using the UVES spectrograph on the Very Large Telescope. Initial simulations by Aigrain et al. (2007) predicted that there would be 4.7 EBs and zero transiting planets in our data.

These observations are part of a larger photometric survey of 9 young ($\lesssim 200$ Myr) open clusters covering a wide range of ages and metallicities (the Monitor project²; Hodgkin et al. 2006 and Aigrain et al. 2007).

1.4 Methods

We developed an automated method to search for occultations in the light curves generated from our NGC 2362 observations.³ In particular, we attempt to remove the significant spot-induced variability displayed by many of our young and late-type targets. As transits and eclipses are essentially the same from a detection standpoint, and cannot always be distinguished from the light curve alone, we detect both types of events among our candidates. We defer the discussion of the EB candidates to a later paper. Here we focus on our transit candidates, for which spectroscopic follow-up observations, to confirm cluster membership and ascertain the source of the occultations by measuring the mass of the occulting body, are underway.

We then perform extensive Monte Carlo simulations to evaluate our sensitivity to planets of different radii and periods around stars of different masses in the cluster, and use these simulations to place upper limits on the incidence of hot and very hot Jupiters (HJs and VHJs) at 5 Myr. These upper limits represent constraints on HJ incidence at an age of less than 10 Myr, when any HJs should have recently finished migrating toward their host star. They therefore constitute an important measurement for constraining planetary formation and migration time-scales.

1.5 Organisation of Paper

The remainder of this paper is structured as follows: the data reduction process is discussed in Section 2, and our method of cluster membership selection is presented in Section 3. The technique used to search for occulting systems and the resulting candidates are described in Section 4. The Monte Carlo simulations and the derived upper limits on the fraction of stars in NGC 2362 with short period planets, are discussed in Section 5. Here we also compare our sensitivity and results to other transit surveys that have targeted stellar clusters. Finally, we present our conclusions in Section 6.

² <http://www.ast.cam.ac.uk/research/monitor/>

³ From this point forward, when we refer to eclipses we specifically mean the eclipse of one star by another star or brown dwarf, while transits only refer to the case of a planet transiting a star. We use the term occultation in a more general sense to include both of these phenomena, but to also include all situations where the flux from a star has been reduced because some other body has passed in front of the stellar disc.

Night	Frames/night	Start	Finish
1	50	406.03573	406.29499
2	47	407.03439	407.28675
3	42	408.03985	408.30530
11	35	416.04713	416.24360
12	41	417.02969	417.24706
13	42	418.04069	418.24918
323	24	728.21098	728.35062
326	30	731.21755	731.36089
328	20	733.27306	733.36723
330	30	735.20998	735.36427
331	32	736.20901	736.36480
332	29	737.21096	737.36434
333	31	738.21689	738.36825
336	31	741.21493	741.36774
359	62	764.04498	764.33686
360	49	765.03671	765.33456
361	61	766.03490	766.32738
362	72	767.03074	767.33916

Table 1. Summary of photometric observations of NGC 2362. Night is the night of observations relative to the first night of observations. Start and Finish are the beginning and end of the nightly observations, respectively, given in HJD - 2453000.5.

2 OBSERVATIONS AND DATA REDUCTION

Photometric monitoring data were obtained using the CTIO 4m Blanco telescope, with the Mosaic-II imager, during 18 nights from February 2005 to January 2006. This instrument provides a field of view of $\sim 36' \times 36'$ (0.37 deg^2), using a mosaic of eight $2k \times 4k$ pixel CCDs, at a scale of $\sim 0''.27$ per pixel. A summary of our observations, including the number of frames per night as well as the start and finish time for each night, is given in Table 1.

Our observations consist of a series of 75 s *i*-band exposures with an average cadence of ~ 6 min. We also obtained a few longer images in the *V*-band (3×600 s) in photometric conditions for the production of a colour magnitude diagram (CMD). Our observations are sufficient to give 1% or better photometric precision per data point from saturation at $i \sim 15$ down to $i \sim 19$, as seen in Figure 1. This range corresponds to G through mid-M spectral types at the age and distance of NGC 2362.

For a full description of our data reduction procedure see Irwin et al. (2007a). Briefly, after we corrected for crosstalk between the detector readouts, we followed the standard CCD reduction scheme of bias correction, flat-fielding, and astrometric calibration before photometric calibration as described in Irwin & Lewis (2001). Following this we generated a *master catalogue* for the *i*-band filter by stacking 20 of the frames taken in the best conditions (seeing, sky brightness and transparency) and running the source detection software on the stacked image. The resulting source positions were used to perform aperture photometry on all of the images, with the final result a time-series of differential photometry. We achieved a per data point photometric precision of ~ 2 -4 mmag for the brightest objects, with RMS scatter $< 1\%$ for $i \lesssim 19$ (see Figure 1).

Our source detection software flags any objects detected as having overlapping isophotes as likely blends. This information is used, in conjunction with a morphological im-

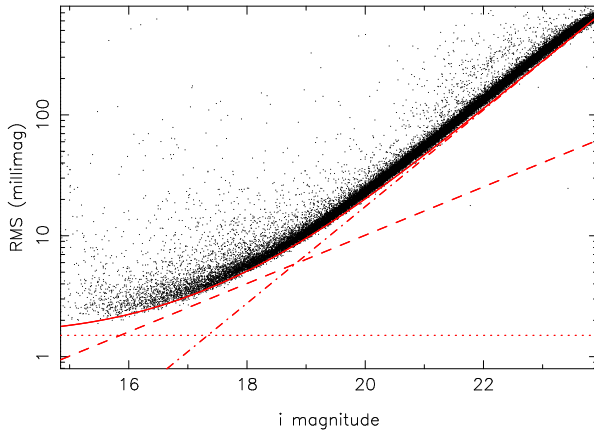


Figure 1. Plot of the rms scatter per data point for the entire series of observations as a function of magnitude for the *i*-band observations of NGC 2362. We include only unblended objects with stellar morphological classifications. The diagonal dashed line shows the expected rms from Poisson noise in the object, the diagonal dash-dot line shows the expected rms from sky noise in the photometric aperture, and the dotted line shows an additional 1.5 mmag contribution added in quadrature to account for systematic effects. The solid line shows the total predicted rms from these effects. This plot shows the rms of our light curves before they have been corrected for seeing.

age classification flag also generated by the pipeline software (Irwin & Lewis 2001), to allow us to identify non-stellar or blended objects in the time-series photometry.

The CCD magnitudes were converted to the standard Johnson-Cousins system using regular observations of Landolt (1992) equatorial star fields in the usual way.

Light curves were extracted from ~ 85 000 objects, 56 000 of which had stellar morphological classification, using our standard aperture photometry techniques (Irwin et al. 2007a). We fit a 2D quadratic polynomial to the residuals in each frame (measured for each object as the difference in magnitude between the current frame and the median taken over all the frames) as a function of position, for each of the eight CCDs separately. We then removed this function to account for variations in transparency and differential atmospheric extinction across each frame. For a single CCD, the spatially varying part of the correction remains small, typically ~ 0.02 mag peak-to-peak.

As a last step there is a small correction applied to all the light curves for seeing-correlated effects. This was done by looking for seeing-correlated shifts in the light curve from its median magnitude. A simple quadratic polynomial was fit to the shift as a function of the full width half max of the stellar images on the corresponding frame. This fit was then subtracted from the light curve. Typically, this fit would reduce the rms of the light curve by < 0.01 mag, however, for the cases that showed the strongest correlations with seeing the reductions in rms would be fairly significant, ~ 0.1 mag.

For the production of deep CMDs, we stacked 20 *i*-band images taken in good seeing and photometric conditions. The long exposure *V*-band frames were stacked before running source detection and the accompanying astrometric and

photometric calibration. The V -band sources were matched against sources in the i -band *master catalogue*, which then enabled us to produce a deep CMD. The limiting magnitudes, measured as the approximate magnitude at which our catalogues are 50% complete were $V \simeq 24.4$ and $i \simeq 23.6$ (Irwin et al. 2007a).

3 SELECTION OF LOW-MASS CANDIDATE MEMBERS

Before we could search for transits we had to identify low-mass cluster members. Lists of candidate members are available in the literature (Moitinho et al. 2001, Dahm & Hillenbrand 2007, Delgado et al. 2006), however, in order to match the field of view of our survey, which is wider than previous surveys of NGC 2362, we elect to use a V versus $V - I$ CMD for candidate membership selection.

3.1 The V versus $V - I$ CMD

The V , $V - I$ CMD used for candidate membership selection is shown in the upper panel of Figure 2. The V and i measurements were converted to the standard Johnson-Cousins photometric system using colour equations from our observations of photometric standard stars (see Eqns. 1-3 from Irwin et al. 2008).

The cluster sequence is difficult to identify by eye, especially when compared to the CMDs of Moitinho et al. (2001) and Dahm (2005). Our survey covered a much larger portion of the sky (0.37 deg.^2 compared to $\sim 0.05 \text{ deg.}^2$ for Moitinho et al. 2001 and $\sim 0.03 \text{ deg.}^2$ for Dahm 2005) and therefore suffers from greater field contamination. Thus, we used a second CMD including only objects within 7 arcmin of τ CMa, defined as the centre of the cluster, to identify the cluster sequence, shown in the lower panel of Figure 2. The 7 arcmin radius was chosen based on a 2σ cut from a Gaussian fit to the radial profile of rotating stars in the field of view. Short period rotators, which are indicative of youth and therefore also cluster membership, were selected from the identifications by Irwin et al. (2008). The presence of rotators at large (> 15 arcmin) distances from the centre of the cluster justifies the use of the entire field of view in our candidate selection process, despite the ensuing high contamination from field objects. We elected to do this because we did not want to miss any transiting planets, which are rare in both the cluster and the field.

We then followed the candidate selection method described in Irwin et al. (2008). Briefly, we manually defined an empirical cluster sequence that follows the sequence visible in Figure 2b. All objects falling between two cuts defined by shifting the sequence right and left (perpendicular to the sequence itself) were then selected as candidate members. This led to the selection of 1813 candidate members over the full range from $V=15.7$ to 26.

To determine model masses and radii for our candidates, the I -band absolute magnitudes of the NextGen model are used, because these are less susceptible to a missing source of opacity, which creates a discrepancy between the models and observations in the $V - I$ colour for $T_{eff} \lesssim 3700 \text{ K}$ (corresponding in this case to $V - I \gtrsim 2.5$

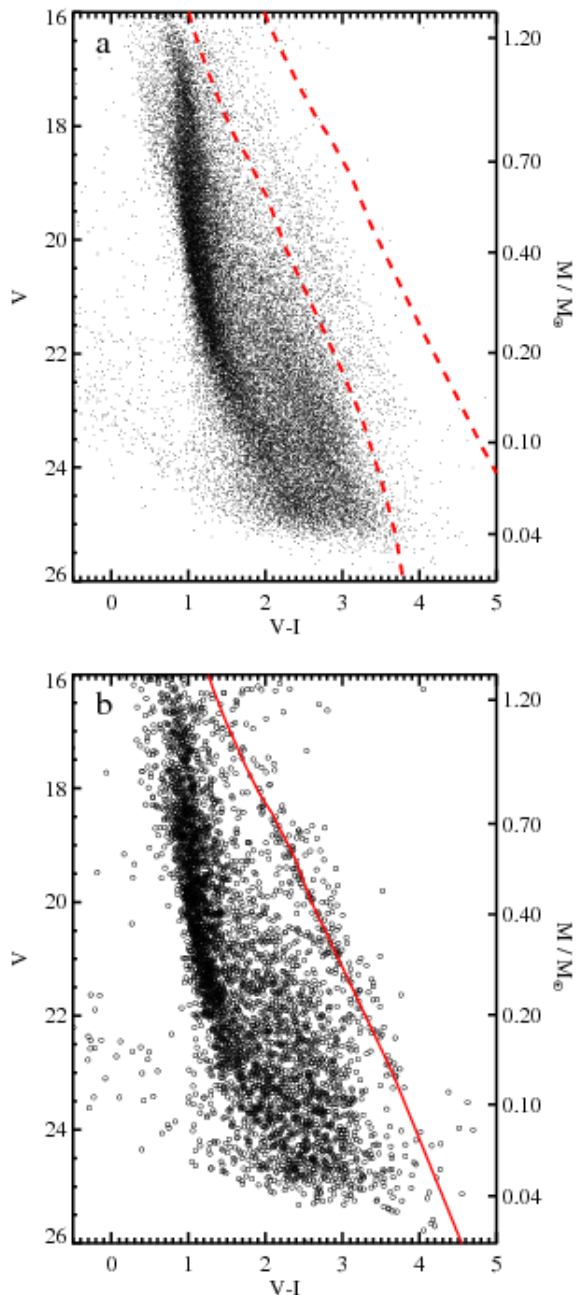


Figure 2. (a) V versus $V - I$ CMD of NGC 2362 from stacked images for all objects with stellar morphological classification. The cluster boundaries, which define candidate membership, are shown as dashed lines (all objects between the lines were selected). The cluster sequence is clearly contaminated by objects in the galactic field. (b) V versus $V - I$ CMD of objects within ~ 7 arcmin of τ CMa, here defined as the centre of the cluster. The 7 arcmin cut was determined by the spatial distribution of rotating stars, as described in the text. The cluster sequence is clearly visible and our empirical sequence is shown as the solid line. The mass scale in both plots is from the 5-Myr NextGen model isochrone (Baraffe et al. 1998), using our empirical isochrone to convert the V magnitudes to I magnitudes, and subsequently obtaining the masses from the I magnitudes due to known problems with the V magnitudes of the models (see Section 3.1).

Baraffe et al. 1998). Therefore the I -band absolute magnitudes give the most robust estimates of mass and radius. Our adopted mass-radius-magnitude relation comes from the procedure described in Aigrain et al. (2007), which combines the NextGen isochrones of Baraffe et al. (1998), with the DUSTY isochrones of Chabrier et al. (2000), and the COND isochrones of Baraffe et al. (2003). This adopted relation covers a mass range from $0.5M_{\text{Jup}}$ to $1.4M_{\odot}$. For the few, ~ 30 , objects that are brighter than the limits of the NextGen models (i.e. $M_I \lesssim 3.9$, or $M_* > 1.4M_{\odot}$) we use the isochrones of Siess et al. (2000) to determine the model masses and radii of those particular candidate cluster members.

3.2 Contamination

Irwin et al. (2008) estimate the level of contamination for the sample of candidate cluster members to be $\sim 65\%$. They caution that their estimate is somewhat uncertain due to the need to use Galactic models. Irwin et al. (2008) also note that spectroscopic follow-up will be needed to make a more accurate contamination estimate. We note that when the range of magnitudes is restricted to those that we search for occultations (see Section 4) the contamination level is slightly reduced to $\sim 60\%$.

4 OCCULTATION DETECTION

While we are nominally searching for transits, our search procedure identifies any light curve with occulting events. Therefore, throughout this section we will discuss our search for occultations, which will inevitably yield a list of transit candidates. After achieving the necessary signal-to-noise, removing systematic trends, and obtaining sufficient coverage and sampling in the data, perhaps the most significant obstacle in any systematic search for occulting systems is the intrinsic variability present in many stars' light curves. Periodic variability, typically due to the rotation of spots on the surface of the star, is a particularly severe contaminant because it leads to regular reductions in the observed flux from the star, which is precisely the behaviour (i.e. occultations) we are trying to identify. Non-periodic variability is also significant in young stars: for instance, a star could change brightness following occultations by or interactions with circumstellar material (see Bouvier et al. 2007 for a discussion of AA Tau, a young star whose photometric variability originates from interactions with its disc). Dahm & Hillenbrand (2007) found an upper limit of $\sim 7\%$ for the fraction of stars with optically thick discs in NGC 2362. Irwin et al. (2008) note the difficulties in determining the fraction of cluster members that rotate, because the rotation sample has a lower contamination level than the remainder of the general candidate cluster members. Applying the same contamination estimates to both populations they estimate a conservative lower limit of $\sim 14\%$ for the fraction of cluster members which are rotating. Irwin et al. (2008) estimates that the actual fraction of cluster members which rotate is $\sim 40\%$ based on the high correlation between rotation and cluster membership. Clearly, there are more rotators than stars with optically thick discs, which is fortunate because rotational variability is easier to filter than non-periodic variability.

The effects of rotation lead to smooth variations in brightness. When this is the dominant source of variability it can be subtracted from the signal without introducing significant additional features into the light curve.

Before we began our search we removed from our sample a number of light curves which were flagged by the data reduction process (Irwin et al. 2007a). Specifically, we removed any light curves that were flagged as saturated and any systems where more than 10% of the data points belonged to low confidence regions in the standard size aperture as flagged by our reduction procedure (Irwin et al. 2007a). We found a few stars which displayed behaviour consistent with saturation were not flagged in the original procedure. Thus, we elected to visually examine the remaining light curves by eye and flag those that were saturated. This led to the removal of an additional 75 objects. Objects that were flagged as blended were not excluded, however, because the reduction procedure of Irwin et al. (2007a) did a sufficient job in correcting the effects of blending such that these objects could be searched for occultations along with the rest of the sample.

We also limited our search with a magnitude cut such that we only examine objects brighter than $I = 19$. We place these cuts based on the limitations of spectroscopic follow-up: the cause of occultations must be confirmed with RV measurements (for a full description of the spectroscopic limitations of this study see Aigrain et al. 2007). Briefly, Aigrain et al. (2007) found that with existing multi-object spectrographs on 8 m class telescopes it would be possible to reach RV precision of ~ 2 km/s down to $I \sim 18$. Our cut of $I = 19$ is thus conservative, yet we point out that Sahu et al. (2006) were able to measure RV variations to ~ 1 km/s for an object with $I = 18.75$ using the UVES echelle spectrograph at the 8-m Very Large Telescope, while Weldrake et al. (2008a) were able to detect a $K = 114$ m/s planet in a 4-day orbit around a K star of $V = 17.4$. We note that any candidates fainter than ~ 18 in I will be extremely difficult to follow-up in order to confirm the origins of the occulting behaviour found in the light curve.

Following the removal of these objects there remained 1180 candidate cluster members to be searched for occultations.

4.1 Variability Filtering

The difficulty with attempting to remove the intrinsic stellar variability from a light curve is that many filtering methods will remove or affect the occultation signal as well as the photometric signal coming from just the star alone. Therefore, the challenge lies in developing a method that successfully disentangles the occultation signal from that of the host star.

Because we find rotation to be the dominant source of variability in the candidate members of NGC 2362, we focused on removing this source of variability. After $k\sigma$ clipping outlying data points in the light curves, we selected rotating stars in our sample by performing a least-squares sine-fit to the time series $m(t)$ (in magnitudes) of every candidate cluster member using

$$m(t) = m_{dc} + \alpha \sin(2\pi t/P + \phi), \quad (1)$$

where m_{dc} is the mean light curve level, α the amplitude, ϕ the phase and P the period of rotation. For the fits m_{dc} ,

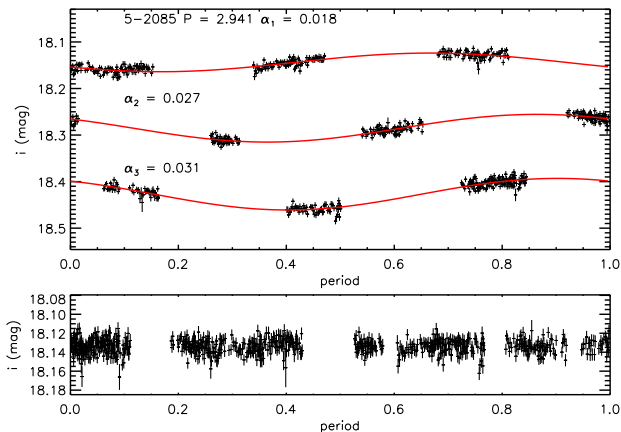


Figure 3. Example rotation fit to star 5-2085. Shown is the light curve and best fit folded over the rotation period (top) and the period-folded sine-subtracted light curve (bottom). The three different observing windows, as described in the text, are shown with 0.15 mag offsets in the top panel. It is clear to see that both the amplitude and phase of the signal from this star change with time. P is the best fit period in days while α_i is the best fit amplitude in magnitudes for each of the observing windows.

α , and ϕ are free parameters at each value of P over a grid of equal logarithmically spaced steps in period from 0.1-181 d (corresponding to half the time between our first and last observations). Our fits adopted a single period, but we allowed the phase and amplitude to change following any gaps in our observations of more than three weeks. We allowed these changes because the size and location of star spots can evolve very rapidly over these time scales in young stars. We fix the period, however, because we would not expect a significant change in the angular momentum of the star in the course of a single year. The output of this procedure is a ‘least-squares periodogram,’ and the best-fitting period is the one with the lowest reduced χ^2 . An example of this fitting procedure is shown in Figure 3, where the data have been folded on the best fit period. From the figure it is easy to see the change in amplitude and phase following long gaps in our observations.

We measured the reduced χ^2 in our light curves before ($\chi_{\nu,\text{flat}}^2$) and after ($\chi_{\nu,\text{fit}}^2$) we subtracted the best sine-fit and selected rotators based on the change in reduced χ^2 :

$$\Delta\chi_{\nu}^2/\chi_{\nu,\text{flat}}^2 > 0.7, \quad (2)$$

where $\chi_{\nu,\text{flat}}^2$ is the reduced χ^2 of the original light curve with respect to a constant model, and $\Delta\chi_{\nu}^2$ is the change in reduced χ^2 following the fit. We also required that $\chi_{\nu,\text{fit}}^2 < 60$ for an object to be classified as a rotator. We acknowledge that a reduced χ^2 of 60 is quite large, however, we find that these systems ($\chi_{\nu,\text{fit}}^2 \sim 60$) display periodic variability. The large value of χ^2 is the result of extremely high signal-to-noise data and slight departures from the modelled behaviour of Eqn. 1. The upper limit for $\chi_{\nu,\text{fit}}^2$ was selected because we found that Eqn. 1 was a poor model for all objects above this threshold. Figure 4 shows $\Delta\chi_{\nu}^2$ plotted against $\chi_{\nu,\text{fit}}^2$, and highlights the systems which were selected as rotators.

The empirically determined cutoff in Eqn. 2 is more

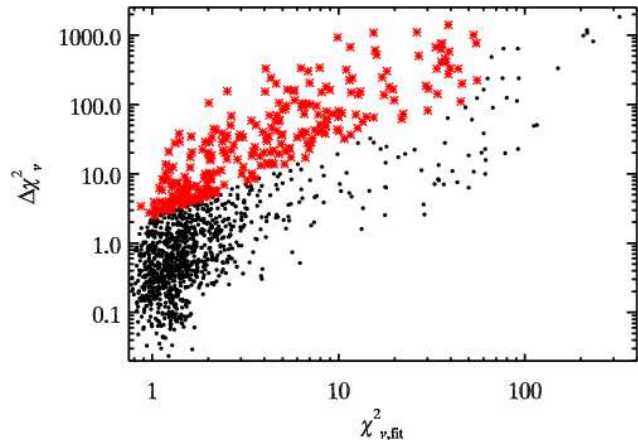


Figure 4. $\Delta\chi_{\nu}^2$ as a function $\chi_{\nu,\text{fit}}^2$ for all candidate cluster members in our sample. The stars highlight the systems that were selected as rotators.

stringent than the initial cut used in the Monitor rotation papers (Irwin et al. 2006, Irwin et al. 2007b, and Irwin et al. 2008). Those papers employ visual inspection of each light curve to remove any objects without clear periodic variability from their sample. Therefore, their samples are more complete. We wish to avoid visual inspection, however, in order to remove human interaction from our selection procedure. As noted by Burke et al. (2006), a clear set of detection criteria that do not rely on human input are extremely important for establishing the actual sensitivity of a survey to planetary transits using Monte Carlo simulations. Therefore we chose not to add a step with visual inspection. We do find that there is generally good agreement between our sample and the one in Irwin et al. (2008), except for the slowest rotators. Irwin et al. (2008) use data from only a single observing season, so they are not sensitive to periods $\gtrsim 24$ days. We also note that our classification scheme leads to some objects, whose variability is not the result of star spots, to be misclassified as rotators, as can be seen by the slight build up around 0.5 and 1 days in the period distribution of Figure 5. This build up is caused by low amplitude night edge effects. For the purposes of this study this less than perfect classification scheme is acceptable because the subtraction of the sine-fits was designed to remove periodic variability of a non-eclipsing nature.

Our goal was to identify any objects which clearly displayed periodic variation of a relatively long temporal signature while excluding those with high-frequency events where the reduced χ^2 would be significantly improved by a sine-fit (i.e. objects with multiple eclipses). We wanted to test that our classification scheme did not identify transits as rotation. To do this we took a sample of our flattest light curves, selected for their low χ^2 ($\chi_{\nu,\text{flat}}^2 < 1.5$) and low dispersion in median flux for each observing season, and inserted transits according to the formalism of Mandel & Agol (2002) using the limb-darkening coefficients of Claret (2000). The planet radius and orbital period were chosen randomly over the same grid as that used in the simulations in Section 5. The orbital inclination and epoch were chosen such that we would have observed at least a portion of one transit. We then ran the rotation test described above and we found

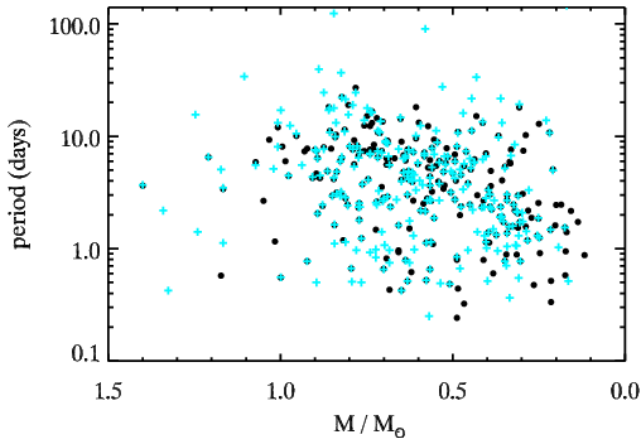


Figure 5. Rotation period versus mass for the candidate cluster members classified as rotators. The blue crosses show those objects classified as rotators in this paper. The large black points show rotators as identified by Irwin et al. (2008). Irwin et al. (2008) only use a portion of the data, so they are not sensitive to periods greater than ~ 24 days. We note that not every cross represents a rotator, especially the excess of objects at ~ 0.5 and ~ 1 d (due to night-edge effects). Other discrepancies between the two samples are likely the result of different windows of observation, such that in some stars spot activity was likely low during the subset of the data that Irwin et al. (2008) examined.

these objects to be misclassified as rotators in $< 0.1\%$ of our test cases. This extremely low rate of false classification allowed us to proceed with confidence that we were not removing occultation signals from our light curves. We were not worried about misclassifying EBs because we found that the removal of a sine curve from an EB light curve left large residuals which were detected by our occultation search algorithm.

Following this procedure we detected rotation in 268 stars, or roughly 23% of the candidate cluster members in our sample. In the objects where rotation was detected we subtracted the best sine-fit from the light curve and searched for occultations in the same manner used for non-rotators described below.

Aigrain & Irwin (2004) propose a number of alternative methods for filtering intrinsic stellar variability without removing the signal from an occultation. We attempted to use their least-squares filtering method and non-linear filtering method but we found these removed the signal from even the deepest eclipses. Aigrain & Irwin (2004) designed these methods for space based occultation surveys, and caution that their procedures are likely only valid for observations which are continuous on time scales \gg a typical occultation. Unfortunately this is rarely, if ever, the case with ground based surveys and we confirm their initial forewarnings.

Lastly, we also attempted to model the variations using the formal spot model of Dorren (1987). We found this method to be far too computationally intensive for an automated procedure, while the least-squares sine-fit serves as a good proxy to the full spot model.

4.2 Noise Properties

Before we began our search for occultations we examined our light curves for the presence of correlated, or red, noise. Ground based surveys have been shown to suffer from red noise (see Pont et al. 2006 for a very detailed discussion, and the typical red noise levels in several existing surveys), which invariably makes it more difficult to detect occulting objects. This correlated noise means that the uncertainty in data binned over n points decreases slower than in the uncorrelated, or white, noise case, where the uncertainty in binned data is $\propto 1/\sqrt{n}$.

Our search for occultations is based on a Box Least Squares (BLS) fit, where the box represents a short time scale periodic decrease in the mean flux from the star. Therefore correlated noise on the same time scale as an occultation can lead to a large detection statistic for every light curve, even those which are spurious. A large detection statistic in every light curve necessitates an extremely large detection threshold, meaning that only the most significant occultations are followed up, while shallow occultations or light curves with only a few occultation data points are not detected. Pont et al. (2006) showed that it is possible to modify the standard white noise detection statistic to account for correlated noise, however, thereby eliminating many of the spurious candidates.

We characterise the presence of red noise in our survey according to the method outlined in Pont et al. (2006) by examining the flattest light curves (low reduced χ^2 with respect to a constant model) in our sample. These objects, which exhibit little variability, should be dominated by noise. Figure 6 shows the RMS scatter for individual points as a function of magnitude as well as the RMS in 15-adjacent-point averages (which for the sampling of our data corresponds to roughly 2.5 hours, a typical time scale for transiting hot Jupiters), compared to the expected value of the RMS in 15-adjacent-point averages in the presence of white noise. It is clear to see that the expected $1/\sqrt{n}$ decrease in the noise does not apply to most of our light curves. Therefore, an assumption of white noise is unfounded, and any attempt to detect occultations must take this red noise into consideration.

For our survey we find correlated noise at a level of ~ 1 mmag for the brightest stars in our sample. This is on a similar scale to the best ground based surveys discussed in Pont et al. (2006).

4.3 Search for Occultations

Following the removal of periodic variability we searched all the candidate cluster members for occultations using a refined version of the BLS algorithm (Kovács et al. 2002) as designed by Aigrain & Irwin (2004). Aigrain & Irwin (2004) show that the best fit model reduces to finding the inverse variance weighted mean of the observed occultation data points. They test the significance of a detection using the familiar detection statistic S :

$$S^2 = \left(\sum_{i \in I} \frac{d_i}{\sigma_i^2} \right)^2 \left(\sum_{i \in I} \frac{1}{\sigma_i^2} \right)^{-1}, \quad (3)$$

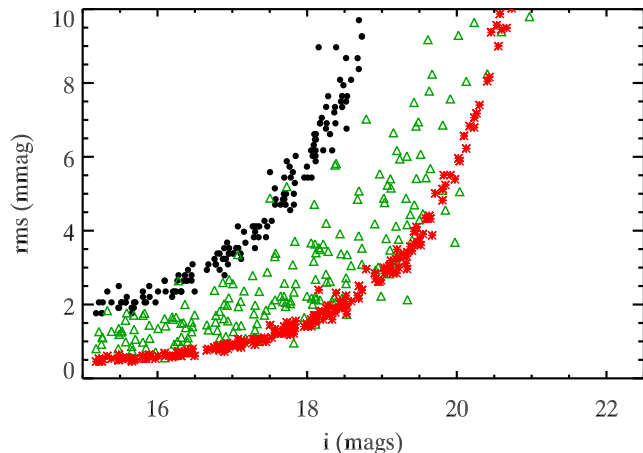


Figure 6. RMS as a function of magnitude for a subset of candidate cluster members in NGC 2362. The filled circles represent the RMS scatter per data point, the triangles the RMS for 15-point averages, and the stars represent the expected values of the 15-point averages assuming white noise. The triangles lie well above the stars indicating the presence of red noise over ~ 2.5 hour time scales. For the brightest stars this appears to be the dominant effect in the noise.

where the sum includes all in-occultation data points i , d_i is the difference in flux between the i th data point and the mean flux of the entire light curve, and σ_i is the uncertainty in the i th flux measurement. Aigrain & Irwin (2004) also show that S^2 is equal to the difference in χ^2 between a flat model and the best fit occultation model of the data. Detections with large S are typically considered the best candidates for spectroscopic follow-up. Aigrain & Irwin (2004) only considers the case of white noise, however, which can lead to many spurious candidates. We discuss the significance of a detection in the presence of red noise below.

We restricted our search to occultations that happen in a period range of 0.4 - 10 days. The upper limit was chosen because Aigrain et al. (2007) show that the time sampling of our observations, combined with the geometric probability of a transit, is insensitive to planets with orbital periods greater than ~ 10 days. The lower limit was selected below the typical boundary of ~ 1 day because we wanted to search for systems with extremely short periods, and because we wanted to test our sensitivity at these short periods in the simulations described in Section 5. It is important to remember, however, that there are no confirmed planet detections to date with periods less than 1 day. (Sahu et al. 2006 found 5 planetary candidates with periods less than a day, and as low as 0.42 days, however, they remain unconfirmed because they are too faint for follow-up spectroscopy.) We show our transiting system recovery fraction as a function of period and the total number of required transits for a positive detection in Figure 7. The figure gives the probability of 1, 2, or 3 transits being present in the data as a function of orbital period. Transits are considered to be present if there are data within the range of phases $\phi < 0.1W/P$ or $\phi > 1 - 0.1W/P$ where W is the expected transit width and P is the orbital period, i.e. a transit is present if we observe some portion of the central 20% of the transit. Given that ≥ 3 detections are needed to accurately determine the period of a system,

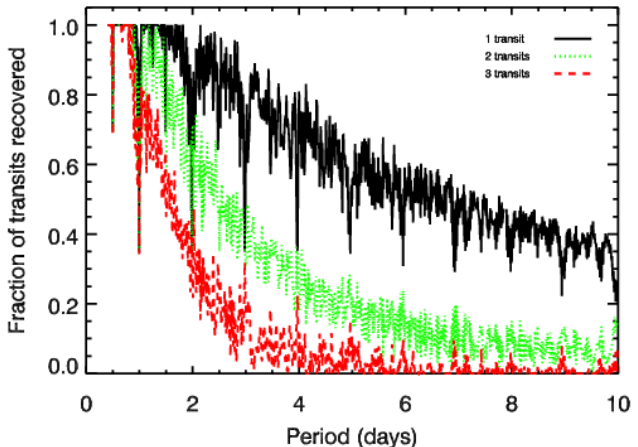


Figure 7. Fraction of transiting systems recovered as a function of orbital period. The results for 1 (top, solid curve), 2 (middle, dotted curve), and 3 (bottom, dashed curve) detected transits are shown.

Figure 7 shows that we can only hope to recover reliable periods for systems with orbital periods $\lesssim 2$ days.

While searching each light curve for the best-fitting occultation model, we also fit for the best brightening occultation model, (defined as an increase in brightness, rather than decrease as is the case for an actual occultation) as described in Burke et al. (2006). This secondary fit has little impact on the numerical efficiency of the fit, because the algorithm simultaneously searches for the greatest reduction in χ^2 in terms of both brightening and dimming. We have no reason to believe that objects with correlated noise on the time scale of an occultation or non-periodic variable objects not selected by the method described in Section 4.1 preferentially show correlated decreases, rather than increases, in flux. On the contrary, one would expect that for these cases both an occultation and brightening could provide good models to the data. Therefore, we use the ratio of the improvement in χ^2 for an occultation model to a brightening model to discriminate against non-eclipsing objects by requiring $\Delta\chi^2/\Delta\chi^2_- > 3$, where $\Delta\chi^2$ is the improvement in χ^2 using an occultation model and $\Delta\chi^2_-$ is the improvement in χ^2 relative to a brightening model.

Figure 8 shows a plot of $\Delta\chi^2_-$ against $\Delta\chi^2$ for every light curve in our sample. The solid line shows the boundary of our requirement $\Delta\chi^2/\Delta\chi^2_- > 3$. Objects below the line pass the selection criteria and are modelled significantly better by an occultation than by brightening.

We employed the method of Pont et al. (2006) to determine the significance of a detection for each light curve in the presence of red noise. They show that the detection statistic, S_{red} in a light curve with red noise can be found without a fit to the individual white and red noise components. We briefly summarise the procedure here: first we found the best fit solution assuming white noise (this is equivalent to maximising S), then we masked points in-occultation. We then calculated the mean flux over a sliding interval equal to the duration of the detected occultation, where the sliding steps are smaller than the interval between flux measurements. We grouped those flux measurements into bins based on the number of data points in the sliding interval, and we cal-

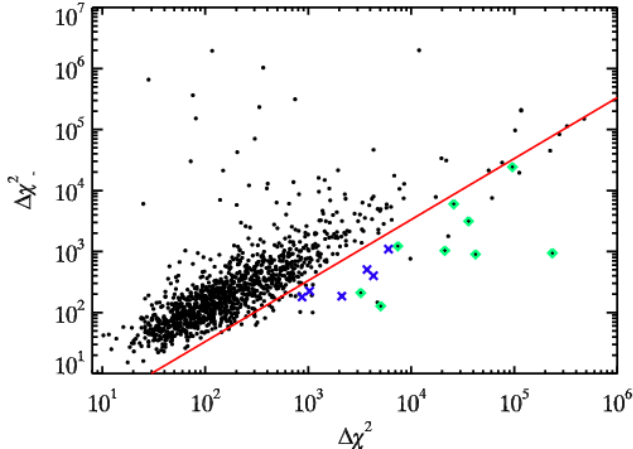


Figure 8. The improvement in χ^2 with respect to a brightening model ($\Delta\chi^2_+$) as a function of the improvement in χ^2 with respect to an occultation model ($\Delta\chi^2_-$) for every searched light curve. The solid line corresponds to $\Delta\chi^2_+/\Delta\chi^2_- = 3$. We require points to lie below the line to be considered occultation candidates. The green diamonds indicate light curves that pass all of our selection criteria. The blue X's are a subset of the green diamonds. In addition to passing all our selection criteria, the blue X's have observed occultation depths that may be compatible with a planetary companion (see Section 4.4).

culated the variance of the flux measurements in each bin. These variances give an estimate to what Pont et al. (2006) call the $V(n)$ function, where $V(1)$ equals the variance in bins with only one point, $V(2)$ equals the variance in bins with two points, and so on. The detection statistic can be measured with $V(n)$ using Eqn. 7 from Pont et al. (2006), reproduced here:

$$S_{\text{red}}^2 = d^2 \frac{n^2}{\sum_{k=1}^{N_{\text{tr}}} n_k^2 V(n_k)}, \quad (4)$$

where d is the depth, n is the total number of data points in-occultation, the sum is over all occultations, and n_k is the number of points in the k th occultation.

After measuring S^2 for each light curve, we determined the corresponding value of S_{red} . We show S_{red} as a function of detector i -band magnitude in Figure 9 for every object in our sample. From the figure it can be seen that we found strong detections ($S_{\text{red}} \gtrsim 6$) over the full magnitude range of our observations. The fact that there is no bulk trend in S_{red} as a function of magnitude shows that S_{red} takes into account any residual correlated noise, which is typically magnitude dependent. The triangles show objects classified as rotators following the procedure in Section 4.1. Figure 9 indicates that our filtering method is successful, as the vast majority of the rotators have detection statistics consistent with non-eclipsing light curves. A plot of S_{red} as a function of best fit period can be seen in Figure 10. We find a large over-density of points at a period of 0.5 days. A histogram of the best fit period for every object shows a high frequency at 0.5 and 1 days. Visual inspection of these light curves shows a systematic effect where slight changes in the median flux (~ 0.005 mag) from one observing season to another can be fit extremely well with periods of ~ 0.5 or ~ 1 days. We are not entirely certain why the flux changes from season to

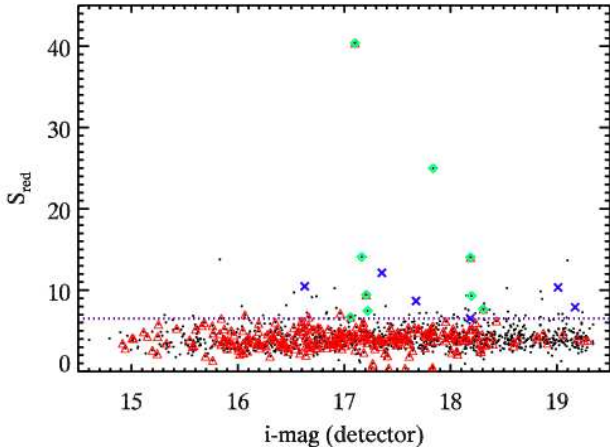


Figure 9. Detection statistic accounting for red noise as a function of CCD i -band magnitude for all candidate cluster members brighter than $I = 19$ (black dots). Objects with large values of S_{red} , which occur over the full magnitude range of our observations, indicate our best occultation candidates. The red triangles show stars classified as rotators. The dashed horizontal line shows our adopted threshold in S_{red} . Stars above the line meet the criteria of the threshold. The green diamonds and blue X's are the same as Figure 8.

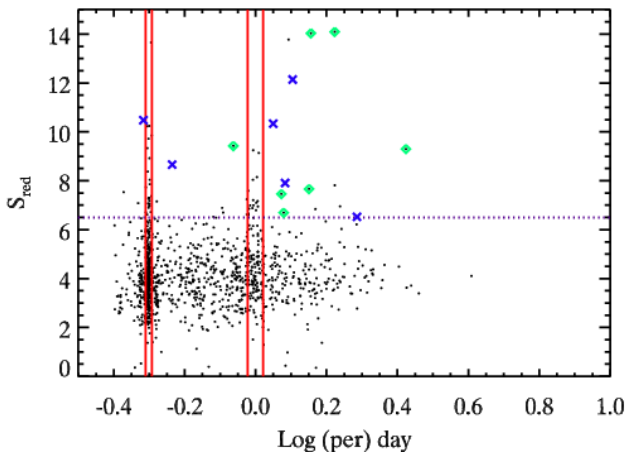


Figure 10. S_{red} as a function of best fit occultation period for all candidate cluster members in our sample. The vertical lines show regions of detected periods that are excluded to remove false positives, as described in the text. The dashed horizontal line shows our adopted threshold in S_{red} . Stars above the line meet the criteria of the threshold. We note that the scale of S_{red} has been reduced, which excludes the two candidate occultation systems at $(i, S_{\text{red}}) \approx (17.1, 40)$ and $(17.6, 25)$ in Figure 9. The green diamonds and blue X's are the same as Figure 8.

season for this subset of objects, but we wish to eliminate these false positives. Therefore, we do not consider any light curves with a best fit period within 1 ± 0.05 and 0.5 ± 0.01 days as detections. The vertical lines in Figure 10 indicate these regions of discarded periods.

4.3.1 Detection Threshold

Following their examination of the effects of correlated noise on the ability of transit surveys to detect planets, Pont et al. (2006) use simulated light curves to show that false positives rarely have values of S_{red} larger than 7. They then argue that the adopted detection threshold will vary from survey to survey, but that it will typically be in the range 7-9.

Following from this, we chose to adopt an inclusive detection threshold of $S_{\text{det}} = 6.5$. Figures 9 and 10 show that very few light curves have $S_{\text{red}} > S_{\text{det}}$, while a histogram of S_{red} for all objects within the allowed range of best fit occultation periods shows very few counts when $S_{\text{red}} > 6.5$. We acknowledge that the selection of this cut will likely increase our false positive rate relative to other transit surveys, however, in our case this may not prove to be entirely detrimental. We investigate the choice of our detection threshold in Section 5, and find that our Monte Carlo simulations corroborate our adopted detection thresholds.

There are a few circumstances that make our situation fairly unique. The first is that the size of the cluster matches the FLAMES field of view (Aigrain et al. 2007). The second is the high scientific value of any transit candidates which turn out to be cluster EBs. Therefore, we can afford to adopt a relatively low threshold and accept more false positives than a typical survey, because (1) we can follow-up many of these candidates at the same time and (2) the detection of any occulting body in the cluster provides an important discovery. In Section 5, we use a series of Monte Carlo simulations to estimate our sensitivity and false positive rate based on our selection of S_{det} .

4.4 Occultation Candidates

15 out of the 1180 candidate cluster members pass all of our selection criteria as occultation candidates. Following depth considerations, planetary transits can be ruled out for all but six of the candidates. For the cases where transits cannot be ruled out very large planets, $> 1.5R_{\text{Jup}}$, would be needed to explain the observed occultation depth.

We estimate the occultation depth for each of the 15 candidates in order to exclude any systems that could not be a dwarf-planet system from our list of transit candidates. The depth is measured by eye in the following way: the minimum flux during occultation is subtracted from the out of occultation flux on the same night. This results in an estimate of the depth in magnitudes. We measure the occultation depth by eye because intrinsic stellar variability makes the best fit depth from our occultation search unreliable. We do not rule out planets in any candidate where the observed occultation depth could be explained by a planet with $R_p \leq 3R_{\text{Jup}}$. This leaves six candidates as possible transits, while the other nine systems remain EB candidates. We defer a discussion of the EB candidates to a later paper. In Table 2 we include the observed occultation depths and corresponding minimum planet radii necessary to explain the occultation. We note that the uncertainty in our estimates of the necessary planetary radius, which relies on stellar evolution models and a visual measurement of the occultation depth, is large. Table 2 also contains the occultation parameters of each of our transit candidates. $\Delta\chi^2/\Delta\chi^2_-$ and S_{red} are the detection statistics discussed in Section 4.3.

star	$\Delta\chi^2/\Delta\chi^2_-$	S_{red}	δ (mag)	R_p (R_{Jup})
3-10048	10.76	12.1	0.05	2.49
3-3739	7.35	10.5	0.03	2.37
3-7559	4.85	6.5	0.05	2.07
5-6469	4.58	8.7	0.03	1.71
6-9484	5.48	7.9	0.17	2.63
7-4723	11.44	10.3	0.15	2.62

Table 2. Fit parameters for candidate transiting systems in NGC 2362. Star is the object identification number from this work. δ is the occultation depth, measured by eye, and R_p is the corresponding planet radius necessary to account for a transit of that depth assuming a central transit.

Table 3 summarises the properties of the six stars where we cannot rule out the possibility of a transit. We include the survey identification number, J2000 coordinates, optical photometry taken at CTIO, *NIR* photometry from 2MASS where available, as well as the model mass and radius for each candidate from our adopted magnitude-mass-radius relation (see Section 3). These estimates of the stellar parameters assume that the observed flux is from a single star, and that there is no occulting body which contributes to the total brightness of the system. If these systems are EBs, then these values serve as upper limits to the mass and radius of the primary star.

In Figure 11 we show the full light curves for each of our transit candidates, as well as a simulated transit included as a reference. We elect to show the entire light curve because in most cases, with the exception of a few, we do not detect enough occultations to accurately determine the period of the system. We show the observed light curves before they have been filtered for variability, because out of occultation variability is indicative of youth, and hence cluster membership. Note that for the model transit the duration is shorter, and the depth is shallower than for our candidate systems. This indicates that there is a good chance that our transit candidates are in fact EB systems.

We note that for each case multi-epoch mid- to high-resolution spectroscopy is going to be needed for RV measurements in order to (1) determine cluster membership via the systemic velocity and (2) confirm whether the observed reductions in flux are the result of an occulting planet or dwarf. Toward these two goals, we will observe NGC 2362 with VLT/FLAMES. In most of these cases additional photometric observations will be needed in order to provide better orbital phase coverage as well as additional detections of the single or partial occultations already observed.

5 RESULTS

5.1 Simulations

We report here on the Monte Carlo simulations designed to characterise the sensitivity of our survey to transits and estimate the false positive rate. We do this by inserting transits into the raw data, correcting for correlations with seeing (see Section 3), and searching the resulting light curves using the same procedure described in Section 4. We consider all simulated light curves to be positive detections if prior to

star	α (J2000)	δ (J2000)	V (mag)	$V - R$ (mag)	$V - I$ (mag)	J (mag)	$J - H$ (mag)	$H - K$ (mag)	M_* (M_\odot)	R_* (R_\odot)
3-10048	7:18:40.95	-24:53:00.9	19.93	1.39	2.85	15.43	0.68	0.15	0.53	1.21
3-3739	7:17:51.68	-24:53:03.3	19.12	1.30	2.76	14.95	0.65	0.34	0.73	1.41
3-7559	7:18:21.73	-24:55:04.2	20.67	1.32	2.76	16.49	1.17	0.23	0.32	0.95
5-6469	7:19:34.23	-25:11:28.6	20.44	1.43	3.06	15.69	0.64	0.22	0.44	1.11
6-9484	7:19:56.21	-25:02:22.2	22.13	1.58	3.28	0.18	0.71
7-4723	7:19:24.32	-24:54:05.4	21.99	1.62	3.30	0.20	0.75

Table 3. Candidate transiting systems in NGC 2362. Star is the object identification number from this work. α and δ are the RA and DEC, respectively. V , $V - R$, and $V - I$ are optical photometry measurements from this work. J , $J - H$ and $H - K$ are IR measurement from 2MASS, where available. M_* and R_* are the model mass and radius, respectively, using our adopted magnitude-mass-radius relation, and assuming the candidate is being occulted an object or material which does not contribute to the total brightness of the system.

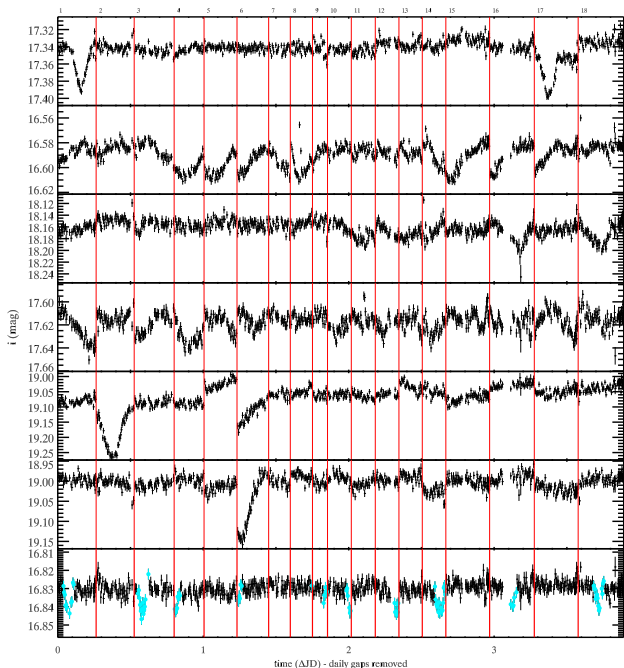


Figure 11. Full light curves for the six stars where we could not rule out the planetary hypothesis. From top to bottom: 3-10048, 3-3739, 3-7559, 5-6469, 6-9484, 7-4723. The bottom panel shows a light curve with an inserted transit (see Section 5). The transits have been highlighted relative to the out-of-transit data. Note that the simulated transit is typically shorter in duration and shallower than the events shown above. Gaps in our observations have been removed and are indicated by the vertical lines. For reference the relative night of observation is listed above the corresponding portion of the light curve.

the injection of a transit $\Delta\chi^2_-/\Delta\chi^2_+ < 3$ and/or $S_{\text{red}} < 6.5$, whereas following the insertion of a planet $\Delta\chi^2_-/\Delta\chi^2_+ > 3$ and $S_{\text{red}} > 6.5$. Saturated stars and stars fainter than $I = 19$ were not included in the simulations. We only insert transits into 1171 of the 1180 light curves we initially searched for occultations in Section 4. The 9 stars where we ruled out the planetary hypothesis based on the depth of the occultations were excluded from the simulations, because they have large reductions in flux that would result in positive detections regardless of the shape or size of the inserted transit signal.

We use the simulations to characterise the survey’s sensitivity to HJs. We define the sensitivity, \mathcal{S} , as

$$\mathcal{S} = \frac{n_d}{N_{\text{sim}}}, \quad (5)$$

where n_d is the total number of planetary systems that we detect and N_{sim} is the total number of simulated planetary systems. This represents a measure of our ability to detect planets over the entire range of possible inclinations, not just those planets that transit their host star. From \mathcal{S} , we can determine the expected number of planet detections, following some assumptions about the fraction of stars with planets.

These simulations accurately address the actual signal to noise in our data, the real cadence and observing windows in our data, and, perhaps most importantly, the intrinsic variability present in the light curve of each individual star. This represents an improvement to the simulations in Aigrain et al. (2007), which assume a signal to noise based on the average noise properties of non-variable light curves and ignore the intrinsic variability of individual stars.

When testing the sensitivity of a transit survey it is important to inject realistic transits into the data (Burke et al. 2006). Therefore, we adopt the formalism of Mandel & Agol (2002), which provides a method for calculating analytic transits given the ratio of planet and star radii as well as the geometry of the orbit. Specifically, we use the quadratic limb-darkening model presented in Section 4 of Mandel & Agol (2002). We determine the limb-darkening coefficients from the tables of Claret (2000), and the stellar properties come from the isochrones of the NextGen, DUSTY, and COND models, as described in Section 3. We acknowledge the perils of assuming the validity of the very models we are trying to test, however, without the use of some model to relate absolute magnitude to stellar mass and radius the following simulations would be impossible.

For our simulations we assume circular orbits. Given the relatively low eccentricities of all discovered extrasolar planets orbiting within 0.1 AU, this is a reasonable assumption. For planets with semi-major axis less than 0.1 AU the median eccentricity is 0.04, with a mean eccentricity $< e > = 0.08$, and only two planets with $e > 0.3$.⁴

Each simulation was run using a uniform distribution in \log_{10} period from 0.4 to 10 days, while the epoch was selected randomly from a uniform distribution of orbital

⁴ <http://exoplanet.eu/catalog.php>

phase. Finally we selected an orbital inclination from a uniform distribution in $\sin i$. Transits only occur when the planet passes in front of the stellar disc, i.e. only in cases where

$$(R_* + R_p)/a \geq \cos i, \quad (6)$$

where R_* is the stellar radius, R_p is the planet radius, and a and i are the orbital semi-major axis and inclination, respectively. Therefore, we could choose to select to only simulate the cases where the inserted planet transits the stellar disc. We choose to select i from the full range of orbital inclinations, however, because we want to use the simulations to test our sensitivity to all planets, regardless of whether the planet transits its host star or not. This choice has a negligible effect on the cost of the total computing time. In the cases where the planet does not transit (i.e. i does not satisfy Eqn. 6), or the phase coverage is such that we do not observe any transits, we do not need to run the search procedure as the light curve remains unchanged and the results of the occultation search are the same as those already obtained during the initial search procedure described in section Section 4.

We inserted planets of radii $1R_{\text{Jup}}$ and $1.5R_{\text{Jup}}$ into the light curves. We arrived at the lower planetary radius because $\sim 1R_{\text{Jup}}$ is roughly the lower limit of radii we are sensitive to following the preliminary simulations of Aigrain et al. (2007). We chose the larger radius based on the evolutionary models of Burrows et al. (1997) for extrasolar giant planets. According to Burrows et al. (1997) at an age of 5 Myr planets in the mass range $0.7M_{\text{Jup}}$ to $2M_{\text{Jup}}$ have radius $R_p \sim 1.5R_{\text{Jup}}$, while the largest radius occurs for a Saturn mass planet ($0.3M_{\text{Jup}}$) with $R_p \sim 1.7R_{\text{Jup}}$.⁵

For every star included in the simulations we independently inserted 300 planets with $R_p = 1R_{\text{Jup}}$ and 300 planets with $R_p = 1.5R_{\text{Jup}}$. Specifically, for each iteration of the simulations we would: (1) add a planet to the system with given R_p , i , and a , which comes from the adopted stellar mass and randomly selected period, (2) check to see if Eqn. 6 is satisfied, if it is then (3) insert the transit into the light curve, and (4) check to see if the randomly chosen epoch results in any observed transits. In total this corresponds to the insertion of 708 000 simulated planetary systems of which we searched $\sim 101\,500$ and $\sim 105\,500$ systems with observed transits for the inserted $1R_{\text{Jup}}$ and $1.5R_{\text{Jup}}$ planets, respectively.

5.1.1 False Positives

False positives cannot be identified by a light curve alone. RV measurements, which can determine the planetary nature and cluster membership of any candidates, are needed to fully characterise the fraction of light curves that are in fact false positives. Brown (2003) calculates the expected number of false positives due to stellar companions for transit surveys of the field star population. An analysis similar to that of Brown (2003) adapted to the stellar population in NGC 2362, which is different from field stars, would be desirable, but is considered beyond the scope of this paper.

S_{red}	$\Delta\chi^2/\Delta\chi_-^2$	$1.0R_{\text{Jup}}$		$1.5R_{\text{Jup}}$	
		\mathcal{S}	\mathcal{FP}	\mathcal{S}	\mathcal{FP}
4.5	2.0	0.069	0.025	0.135	0.025
5.0	2.0	0.066	0.022	0.132	0.022
5.5	2.0	0.062	0.020	0.128	0.020
6.0	2.5	0.048	0.011	0.117	0.011
6.5	3.0	0.038	0.005	0.107	0.005
8.0	3.0	0.029	0.003	0.095	0.003
10.0	5.0	0.012	0.002	0.072	0.002
15.0	10.0	0.001	0.000	0.038	0.000

Table 4. Sensitivity, \mathcal{S} , assuming a logarithmic distribution in orbital periods, and the upper bound to the fraction of false positives (\mathcal{FP}) as a function of planet radius. Note that \mathcal{S} and \mathcal{FP} are not directly comparable because the quoted values of \mathcal{S} assume every star has a HJ.

5.1.2 Sensitivity as a Function of Detection Threshold

We now evaluate our selected thresholds based on the results of our simulations. In Table 4 we summarise the sensitivity and maximum false positive fraction for a number of different thresholds in S_{red} and $\Delta\chi^2/\Delta\chi_-^2$ for both $1R_{\text{Jup}}$ and $1.5R_{\text{Jup}}$. As noted above, we cannot determine the number of false positives from the light curves alone. If we assume that there are no transiting planets in our data, then we can, however, determine an upper bound to the number of false positives. This upper bound is determined by assuming that all systems which pass the detection criteria are considered false positives:

$$\mathcal{FP} = \frac{n_{\text{cand}}}{1171}, \quad (7)$$

where \mathcal{FP} is the upper bound on the number of false positives, n_{cand} is the number of systems that pass all the selection criteria, and 1171 is the total number of searched systems.

The quoted values of \mathcal{S} assume that every star has a HJ, which means the number of detections relative to the number of false positives cannot be found by dividing \mathcal{S} by \mathcal{FP} . To find this ratio \mathcal{S} would have to be multiplied by the fraction of stars with a HJ, or $\sim 1\%$ (Gaudi et al. 2005; we caution that this result is limited to the solar neighbourhood and may not apply to a cluster at the distance of NGC 2362, where the formation environment may be significantly different than that in the solar neighbourhood).

What Table 4 clearly shows is that there is very little improvement in the sensitivity when the S_{red} threshold is lowered below 5.5, while at the same time \mathcal{FP} grows relatively quickly. At the same time, to obtain $\mathcal{FP} < 0.1\%$ would require the selection of very large detection thresholds. Given the relatively small number of cluster stars in this survey, such a large threshold would be inadvisable. Reducing the thresholds from these large values to $S_{\text{red}} \sim 6$ and $\Delta\chi^2/\Delta\chi_-^2 \sim 3$ results in the largest gains in \mathcal{S} relative to the increase in \mathcal{FP} . We arrive at our final thresholds of $S_{\text{red}} = 6.5$ and $\Delta\chi^2/\Delta\chi_-^2 = 3$, because reducing each of those thresholds by 0.5 creates additional occultation candidates whose variability is clearly not the result of eclipses or transits.

If we assume that 1% of stars have a HJ then the values quoted in Table 4 are somewhat discouraging. This would

⁵ <http://zenith.as.arizona.edu/~burrows/>

mass (M_{\odot})	radius (R_{\odot})	$\frac{1.0R_{\text{Jup}}}{\mathcal{S}}$	$\frac{1.5R_{\text{Jup}}}{\mathcal{S}}$
< 0.3	< 0.92	0.048	0.114
0.3 - 0.5	0.92 - 1.18	0.038	0.104
0.5 - 0.7	1.18 - 1.38	0.027	0.102
> 0.7	> 1.38	0.037	0.109

Table 5. Sensitivity as a function of stellar mass and radius. The mass and radius are determined from our adopted magnitude-mass-radius relation as described in the text. \mathcal{S} is the sensitivity for each range of masses.

mean that, given our adopted thresholds, for a large survey in order to detect 1 planet at $1R_{\text{Jup}}$ and $1.5R_{\text{Jup}}$ we would have ~ 13 and ~ 5 false positives, respectively. This is somewhat abated considering this cluster lies within a single FLAMES field of view, meaning that the telescope time needed for spectroscopic follow-up is essentially independent of the number of candidates.

5.1.3 Sensitivity as a Function of Stellar Mass

As noted previously, the presence of a planet cannot be inferred from a light curve alone. Given that consistent RV variations are needed to confirm a planet, it would be very useful to understand our sensitivity as a function of stellar mass for stars in the cluster. Our ability to detect planets in NGC 2362 via RV variations is strongly dependent on the mass of the host star (Aigrain et al. 2007). Assuming a Jupiter mass planet, the greatest signal in RV variations is going to occur for the lowest mass stars, however, these stars are also going to be the faintest in the cluster meaning it will be difficult to obtain spectra with sufficient signal-to-noise to detect the RV variations. While moving to higher mass stars will dramatically improve the signal-to-noise in a single spectrum it will cause a significant reduction in the RV amplitude, again assuming a Jupiter mass companion. This will make it difficult to detect a planet. Thus, an understanding of the sensitivity as a function of stellar mass becomes extremely important when determining which systems to follow-up for this cluster and for the Monitor project as a whole.

In Table 5 we summarise the sensitivity to HJs as a function of stellar mass. We also show the corresponding radii from our adopted magnitude-mass-radius relation. Somewhat surprisingly, Table 5 shows that we are more likely to recover a planet around a smaller star. This is surprising because the stars with the lowest pre-transit rms are all at the bright (and hence higher mass) end of the cluster. This implies that the effect of reduced stellar radii is more important than a low rms when trying to detect transits. This confirms the initial findings of Aigrain & Pont (2007), who examined the detectability of transits in a hypothetical cluster. Aigrain & Pont (2007) found that when red noise is considered it becomes more difficult to detect planets around the brighter cluster members even though they have a smaller rms. Our results suggest that small stellar radii may be the most important factor in detecting transits given that our survey is most sensitive to planets orbiting stars with mass $< 0.3M_{\odot}$ and radius $< 0.92R_{\odot}$.

5.2 Expected Number of Hot Jupiter Detections

Using the Monte Carlo simulations described above we estimate the expected number of detectable short period planets in NGC 2362. Many factors must be accounted for in order to estimate the number of expected detections, including: the frequency of HJs, the total number of candidate cluster members and the contamination from field stars, the geometric transit probability as a function of period, and our recovery rate as a function of period. We note that the relatively small number of cluster members in NGC 2362 means that a null result in NGC 2362 does not carry much significance.

We begin by assuming that the frequency of large, short period planets is the same as that found in the solar neighbourhood. Gaudi et al. (2005) identify two empirically defined populations of planets with periods $\lesssim 10$ days. Following from their work we assume the frequency of hot Jupiters, O_{pl} , with periods of 3-10 days, to be 1%. Strictly speaking, the estimates from Gaudi et al. (2005) include only planets with periods up to 9 days. We extend their estimate to 10 days without loss of generality. The frequency of HJs in the other population with periods < 3 days, which Gaudi et al. (2005) refer to as VHJs, is $\sim 0.15\%$. This is then multiplied by the number of candidate cluster members, N_* , and the probability of membership, P_{memb} , to arrive at the expected number of HJs in our data set. The number of HJs is not randomly distributed in orbital period. The actual distribution of orbital periods is currently ill constrained, though it likely depends on the physical parameters of the system in which the planet is formed. In order to calculate the number of expected detections we must make some assumption about the period distribution. Therefore, we assume a uniform logarithmic distribution in orbital period. We then separate the expected number of HJs into equal size bins in $\log(\text{period})$ space and calculate the number of planets in each period bin i , which we then sum to arrive at

$$N_{\text{det}} = \sum_{i=m}^n N_{\text{pl}}(\text{per}_i), \quad (8)$$

with

$$N_{\text{pl}}(\text{per}_i) = N_* P_{\text{memb}} O_{\text{pl}} f_{\text{pl}_i} \mathcal{S}_i \quad (9)$$

where N_{det} is the total number of detectable HJs present in the data set, $N_* P_{\text{memb}}$ is the number of cluster members we observed, O_{pl} is the frequency of HJs in the solar neighbourhood, f_{pl_i} is an estimate of the fraction of the total number of HJs in bin i based on a logarithmic distribution of orbital periods, and \mathcal{S}_i is our sensitivity to planets in the i th period bin. Our final assumption is that there are no HJs with periods less than 1 day, because to date there have been no RV confirmed planets found with periods < 1 day.

The resulting expected distribution of HJs is shown in Table 6. We find that we would only expect to detect 0.19 HJs in NGC 2362, which is consistent with a null detection. The values quoted in Table 6 assume that HJs orbiting young stars have bloated radii of $1.5R_{\text{Jup}}$. If instead we assume that these planets all have radii of $1.0R_{\text{Jup}}$ then the sensitivity is reduced and the expected number of detectable HJs in our data is reduced to 0.038. Under either circumstance, it is clear that we would not expect to find any HJs in our data.

Period (days)	F_{pl_i}	\mathcal{S}_i	$N_{\text{pl}}(\text{Per})$
0.4-1	0.00	0.228	0.000
1-3	0.71	0.094	0.066
3-10	4.72	0.027	0.126

Table 6. Number of expected detectable, transiting planets in NGC 2362. We have separated the results into 3 different populations based on orbital period. F_{pl_i} is the expected number of HJs in our data in the corresponding period range. \mathcal{S}_i is the sensitivity to $1.5R_{\text{Jup}}$ HJs, as determined by our Monte Carlo simulations. $N_{\text{pl}}(\text{Per})$ is the expected number of transit detections at each period.

5.2.1 Upper Limits on the Planetary Fraction in NGC 2362

Given our null detection (assuming that none of our candidates are planetary transits, which has yet to be confirmed) we can place upper limits on the fraction of stars in NGC 2362 with a HJ. We do this by assuming that all stars in the cluster have a HJ, and then calculate the corresponding number of expected detections based on the results of our Monte Carlo simulations. Following from there we can evaluate the statistical significance of a null result given the number of expected detections.

Based on RV surveys of the solar neighbourhood, we know that not every star has a HJ (Gaudi et al. 2005). The actual number of stars with detectable HJs will be a Poisson distribution with mean $\mu = f_p N_{\text{det}}$, where f_p is the actual fraction of stars with HJs and N_{det} is the expected number of detections assuming all stars have a HJ. For a Poisson distribution the probability of n detections given a mean μ is

$$P(n; \mu) = \frac{e^{-\mu} \mu^n}{n!}. \quad (10)$$

For our null result $n = 0$, which when we substitute into Equation 10 yields

$$P(0; f_p N_{\text{det}}) = e^{-f_p N_{\text{det}}}. \quad (11)$$

To obtain an upper limit on f_p at significance α we require that

$$\alpha \geq P(0; f_p N_{\text{det}}). \quad (12)$$

When we substitute Equation 11 into Equation 12 we arrive at

$$f_p \leq \frac{-\ln \alpha}{N_{\text{det}}}, \quad (13)$$

which allows us to place an upper limit on f_p at any significance α (or confidence level $1-\alpha$). For example, if one expects to detect 3 planets, then there is a 5% chance of detecting zero planets from Poisson statistics alone (Eqn. 11). Equivalently, to convert a null detection to a statistical result at 95% confidence or greater, the expectation value of the number of planets detected should be 3 or greater.

In Table 7 we show the derived upper limits on f_p for $\alpha = 0.05$ and 0.01 (corresponding to confidence levels of 95% and 99%, respectively) for HJs with $R_p = 1.0R_{\text{Jup}}$ and $1.5R_{\text{Jup}}$. We quote upper limits for two different period ranges: 1-3 d, and 3-10 d. In order to calculate the upper

R_p (R_{Jup})	N_{det}	Period range (days)	U. L. on f_p at $\alpha = 0.05$	U. L. on f_p at $\alpha = 0.01$
1.0	5.75	1.0 - 3.0	0.521	0.801
1.0	1.03	3.0 - 10.0	1.000*	1.000*
1.5	21.15	1.0 - 3.0	0.142	0.218
1.5	6.61	3.0 - 10.0	0.453	0.697

Table 7. Upper limits on the fraction of stars with HJs. R_p is the planet radius. N_{det} is the expected number of detections if every star has a HJ. f_p is the fraction of stars with HJs in the given period bin, and α is the significance level of the upper limit on f_p . *For the case of 3 - 10 day $1R_{\text{Jup}}$ planets we cannot place upper limits below every star in the cluster having a HJ in this period range.

limits in each period bin we assume that every star has one planet of radius R_p . We then determine the number of stars with a HJ in a given bin, assuming a uniform logarithmic distribution, and multiply this by the sensitivity, \mathcal{S}_i , in the given bin to arrive at N_{det} . The most significant upper limits we find are at $\alpha = 0.01$, where if HJs at ~ 5 Myr are about $1.5R_{\text{Jup}}$ then the upper limit on short (1-3 days) period HJs is 22% while the upper limit on HJs with periods between 3-10 days is 70%. These limits provide strong evidence against the 'survival of the lucky few' scenario, where most planets migrate into their host star and only those that form just prior to the dispersal of the disc survive, as discussed in Aigrain et al. (2007). We note that if HJs at this age tend to be closer to $1R_{\text{Jup}}$ we cannot place reliable constraints on f_p .

5.3 Discussion

Given the number of cluster stars (~ 475), the number of hours observing (~ 100), and the faintness of many of the cluster members it is unlikely that we would have detected a planet in NGC 2362. The failure to detect a planet is unsurprising based on our simulations, and the simulations of Aigrain et al. (2007), which predicted zero detectable planets in our data for this cluster (again, we are assuming that none of our transit candidates are in fact transiting planets, which remains to be confirmed). In fact, the detection of a planet would have been more inconsistent with the expectations than a non-detection, and would likely provide strong evidence for a greater incidence of planets around young stars than MS stars.

5.3.1 Comparison with Other Cluster Surveys

There have been many surveys searching for planetary transits in star clusters (see Wel Drake 2007 for a review). These surveys are unique relative to the many shallow, wide-field transit surveys, because they examine stars of a known age and metallicity. Therefore any planets or low mass EBs found in these clusters can be used as observational constraints on stellar environments and their evolution.

These cluster surveys also present an opportunity to place upper limits on HJ incidence at a number of stellar ages. Unfortunately, few of these surveys have actually calculated upper limits on f_p , but we can compare our results with those that have. Burke et al. (2006) surveyed the ~ 1

Gyr cluster NGC 1245, and found 95% confidence upper limits for 1-3 day orbits which are a factor of ~ 2 smaller than the upper limits from this work. They find upper limits of 6.4% and 24% for $1.5R_{\text{Jup}}$ and $1.0R_{\text{Jup}}$ HJs, respectively, compared to upper limits of 14% and 52%, respectively, from this work. We report an upper limit for 3-10 day period HJs of 45%, which is lower than the Burke et al. (2006) value of 52% for $1.5R_{\text{Jup}}$ planets. Neither study was able to place meaningful upper limits on the incidence of $1R_{\text{Jup}}$ planets in 3-10 day orbits. Bramich & Horne (2006) were able to place better upper limits on f_p than those found in this study, however, they included both field and cluster stars ($N_* \sim 30000$) in their analysis. Weldrake et al. (2008b) observed 31 000 stars in the globular cluster ω Centauri for 25 nights. These observations allowed them place a 95% confidence level upper limit of 0.1% on $1.5R_{\text{Jup}}$ planets in 1-3 day orbits. Given the significantly larger number of targets in both the Bramich & Horne (2006) and Weldrake et al. (2008b) surveys it is unsurprising that they place more restricting upper limits on f_p .

5.3.2 Extensions to the Remainder of Monitor

We can also explore what happens when we extrapolate our results to Monitor as a whole. Monitor will observe a total of nearly 15 000 young (< 200 Myr) stars, most of which have not yet reached the MS. This significant increase over the number of targets in NGC 2362 will lead to large reductions in the limits on f_p for young stars.

In fact, observations of an additional Monitor target, h & χ Per, which has ~ 7500 cluster members (Aigrain et al. 2007), will lead to a considerable reduction in the limits on f_p for young stars. Assuming the only difference between clusters is the number of observed stars⁶, then we would be able to reduce all the upper limits in Table 7 by a factor of ~ 13 following the observation of h & χ Per. When we consider all the stars to be observed by Monitor we will be able to reduce the limits on f_p by a factor of ~ 26 . For the case of $1.5R_{\text{Jup}}$ planets in 3-10 day orbits this would mean an upper limit of $\sim 2.7\%$.

The above predictions assume that our achieved sensitivity in NGC 2362 will be the same in each of the clusters we have observed. Most of the Monitor targets are both older and less distant than NGC 2362, meaning in these cases we are probing stars with smaller radii and less intrinsic variability. As seen in Section 5.1.3, smaller radii should result in an improved sensitivity. Assuming a sensitivity equal to that in NGC 2362 we can estimate the final upper limits on f_p we would expect from Monitor. These values are summarised in Table 8.

⁶ We note that this assumption is a significant over simplification of the actual situation given that the clusters are at different distances, are being observed with different telescopes, have different noise properties, and are different ages, however, we proceed simply to provide an order of magnitude estimate for the improvement in f_p .

R_p (R_{Jup})	per (days)	f_p ($S = S_{2362}$)
1.0	1-3	0.031
1.0	3-10	0.183
1.5	1-3	0.008
1.5	3-10	0.027

Table 8. Summary of the expected $\alpha = 0.01$ upper limits on the fraction of young stars with HJs following ~ 100 hrs of observations of each of the Monitor targets. R_p and per are the planet radius and orbital period, respectively. f_p is the upper limit on the fraction of stars with HJs assuming that we achieve a sensitivity in all other clusters equal to that which we achieved in NGC 2362.

5.3.3 Future Observational Considerations

Finally, we would like to discuss the limitations of our survey of NGC 2362. We have learned that our sensitivity is largely limited by intrinsic stellar variability and stars with large radii. Both of these limitations could be reduced by observing older clusters: there will be less intrinsic variability while the stellar radii will be smaller given that the stars have had more time to contract toward their MS radius.

Another way to increase the sensitivity of our survey would be to decrease the point-to-point rms and the noise over time-scales equal to or longer than the duration of a transit. Given that the red and white noise properties of our data are dependent on a number of factors, including the detectors, sky noise, and observing conditions to name a few, there is no simple panacea for reducing the noise. However, there is one slight change in observing strategy which would generally reduce the noise (both red, which would have the greatest effect on our brightest targets, and white, which would have the greatest effect on our faintest targets) in the light curves: conducting all observations within a single observing season. Even in many of the light curves with low χ^2 with respect to a flat model we notice small fluctuations, of order 0.01 mag, in the median flux following large gaps in our observations. These shifts are real and not the result of systematics. Making all the observations in a single observing season will remove this slight source of variability from our data and create a greater sensitivity to transits. We also note that this change in strategy would have the added benefit of significantly reducing the computing time necessary to adequately search the light curves for transits using our search algorithm.

6 SUMMARY AND CONCLUSIONS

We have conducted a search for occultations in NGC 2362. We observed the cluster on 18 nights from February 2005 to January 2006 with the Mosaic II imager on the 4m Blanco telescope at CTIO. We achieved an average cadence of ~ 6 minutes, which is sufficient to perform differential photometry and search the data set for any transits. We used a $V, V-I$ CMD to photometrically select 1813 candidate cluster members.

Following the selection of candidate cluster members, we developed a systematic method for searching and identifying occultations in our light curves. This method con-

sisted of two major steps: (1) the identification and removal of intrinsic stellar variability due to rotation, and (2) the search for transits using the occultation search algorithm of Aigrain & Irwin (2004) modified to account for red noise. Following the removal of saturated stars and stars too faint for spectroscopic follow-up, we searched a total of 1180 stars for transits, of which about ~ 475 are expected to be cluster members according to our contamination estimate.

Our search identified 15 light curves with reductions in flux that passed all of our detection criteria. Only six of these systems, however, have observed variability that would be compatible with a planetary companion based on the observed occultation depth. Some of these systems may be cluster EBs, which would help to provide important constraints on the mass and radius, and by extension evolution, of PMS stars.

Using a series of Monte Carlo simulations we predict the number of detectable HJs and find it is consistent with our null result. With 99% confidence we place a limit on the fraction of stars in NGC 2362 with 1-3 d period HJs at $<22\%$, while we limit the fraction with 3-10 d period HJs at $<70\%$, assuming a planetary radius of $1.5R_{\text{Jup}}$. We compare these limits with other cluster surveys and find that we are not as sensitive to transits as other surveys, because we have far fewer targets. The limits for NGC 2362 provide observational constraints on the fraction of stars with HJs at an age < 10 Myr. From the simulations we also know that our sensitivity to transits increases as the stellar radius decreases, a somewhat non-intuitive result, which supports the findings of Aigrain & Pont (2007).

Finally, we examine the prospects of the Monitor project as a whole. If we assume the same sensitivity is achieved for the entire Monitor survey, we will be able to place an upper limit on the number of young stars with a $1.5R_{\text{Jup}}$ HJ at $\sim 2.7\%$, assuming a null detection.

Acknowledgments

Based on observations obtained at CTIO, a division of the National Optical Astronomy Observatories, which is operated by the Association of Universities for Research in Astronomy, Inc. under cooperative agreement with the National Science Foundation. This publication makes use of data products from the 2MASS, which is a joint project of the University of Massachusetts and the Infrared Processing and Analysis Center/California Institute of Technology, funded by the National Aeronautics and Space Administration and the National Science Foundation. This research has also made use of the SIMBAD data base, operated at CDS, Strasbourg, France.

We wish to thank the referee for the thoughtful comments towards improving this paper. AM gratefully acknowledges the support of a Gates-Cambridge Trust fellowship. AM would like to thank Cathie Clarke and Keivan Stassun for their useful comments regarding the content of this paper. JI gratefully acknowledges the support of a PPARC studentship, and SA the support of a PPARC postdoctoral fellowship.

REFERENCES

- Agol E., Steffen J., Sari R., Clarkson W., 2005, *MNRAS*, 359, 567
- Aigrain S., Hodgkin S., Irwin J., Hebb L., Irwin M., Favata F., Moraux E., Pont F., 2007, *MNRAS*, 375, 29
- Aigrain S., Irwin M., 2004, *MNRAS*, 350, 331
- Aigrain S., Pont F., 2007, *MNRAS*, 378, 741
- Baraffe I., Chabrier G., Allard F., Hauschildt P. H., 1998, *A&A*, 337, 403
- Baraffe I., Chabrier G., Barman T. S., Allard F., Hauschildt P. H., 2003, *A&A*, 402, 701
- Bodenheimer P., Lin D. N. C., 2002, *Annual Review of Earth and Planetary Sciences*, 30, 113
- Bouvier J., Alencar S. H. P., Bouvier T., Dougados C., Balog Z., Grankin K., Hodgkin S. T., Ibrahimov M. A., Kun M., Magakian T. Y., Pinte C., 2007, *A&A*, 463, 1017
- Bramich D. M., Horne K., 2006, *MNRAS*, 367, 1677
- Brown, T. M., 2003, *ApJL*, 593, L125
- Burke C. J., Gaudi B. S., DePoy D. L., Pogge R. W., 2006, *AJ*, 132, 210
- Burrows A., Marley M., Hubbard W. B., Lunine J. I., Guillot T., Saumon D., Freedman R., Sudarsky D., Sharp C., 1997, *ApJ*, 491, 856
- Chabrier G., Baraffe I., Allard F., Hauschildt P., 2000, *ApJ*, 542, 464
- Claret A., 2000, *A&A*, 363, 1081
- Dahm S. E., 2005, *AJ*, 130, 1805
- Dahm S. E., Hillenbrand L., 2007, *AJ*, 133, 2072
- Delgado A. J., González-Martín O., Alfaro E. J., Yun J., 2006, *ApJ*, 646, 269
- Dorren J. D., 1987, *ApJ*, 320, 756
- Gaudi B. S., Seager S., Mallen-Ornelas G., 2005, *ApJ*, 623, 472
- Grillmair C. J., Charbonneau D., Burrows A., Armus L., Stauffer J., Meadows V., Van Cleve J., Levine D., 2007, *ApJL*, 658, L115
- Haisch Jr. K. E., Lada E. A., Lada C. J., 2001, *ApJL*, 553, L153
- Hodgkin S. T., Irwin J. M., Aigrain S., Hebb L., Moraux E., Irwin M. J., the Monitor collaboration 2006, *Astronomische Nachrichten*, 327, 9
- Holman M. J., Murray N. W., 2005, *Science*, 307, 1288
- Irwin J., Aigrain S., Hodgkin S., Irwin M., Bouvier J., Clarke C., Hebb L., Moraux E., 2006, *MNRAS*, 370, 954
- Irwin J., Irwin M., Aigrain S., Hodgkin S., Hebb L., Moraux E., 2007a, *MNRAS*, 375, 1449
- Irwin J., Hodgkin S., Aigrain S., Hebb L., Bouvier J., Clarke C., Moraux E., Bramich D. M., 2007b, *MNRAS*, 377, 741
- Irwin J., Hodgkin S., Aigrain S., Bouvier J., Hebb L., Irwin M., Moraux E., 2008, *MNRAS*, 384, 675
- Irwin M., Lewis J., 2001, *New Astronomy Review*, 45, 105
- Kovács G., Zucker S., Mazeh T., 2002, *A&A*, 391, 369
- Landolt A. U., 1992, *AJ*, 104, 340
- Mandel K., Agol E., 2002, *ApJL*, 580, L171
- Moitinho A., Alves J., Huélamo N., Lada C. J., 2001, *ApJL*, 563, L73
- Pont F., Zucker S., Queloz D., 2006, *MNRAS*, 373, 231
- Richardson L. J., Deming D., Horning K., Seager S., Harrington J., 2007, *Nat*, 445, 892
- Sahu K. C. et al., 2006, *Nat*, 443, 534

- Setiawan J., Henning T., Launhardt R., Müller A., Weise P., Kürster M., 2008, Nat, 451, 38
- Siess L., Dufour E., Forestini M., 2000, A&A, 358, 593
- Weldrake D. T. F., 2007, ArXiv e-prints, 709 (astro-ph/0709.4493)
- Weldrake, D. T. F. and Bayliss, D. D. R. and Sackett, P. D. and Tingley, B. W. and Gillon, M. and Setiawan, J., 2008a, ApJ, 675, 37L
- Weldrake D. T. F., Sackett P. D., Bridges T. J., 2008b, ApJ, 135, 649